

Automatic topography of high-dimensional data sets by non-parametric Density Peak clustering

Maria d'Errico,¹ Elena Facco,¹ Alessandro Laio,^{1, 2,*} and Alex Rodriguez^{1, †}

¹SISSA, Scuola Internazionale Superiore Studi Avanzati, via Bonomea 265, I-34136 Trieste, Italy
²ICTP, International Centre for Theoretical Physics, Strada Costiera 11, I-34100, Trieste, Italy

(Dated: March 20, 2022)

Data analysis in high-dimensional spaces aims at obtaining a synthetic description of a data set, revealing its main structure and its salient features. We here introduce an approach for charting data spaces, providing a *topography* of the probability distribution from which the data are harvested. This topography includes information on the number and the height of the probability peaks, the depth of the “valleys” separating them, the relative location of the peaks and their hierarchical organization. The topography is reconstructed by using an unsupervised variant of Density Peak clustering exploiting a non-parametric density estimator, which automatically measures the density in the manifold containing the data. Importantly, the density estimator provides an estimate of the error. This is a key feature, which allows distinguishing genuine probability peaks from density fluctuations due to finite sampling.

Keywords: Clustering | Complex topographies | Non-parametric Density Estimation

I. INTRODUCTION

The rapidly increasing capability to generate data calls for approaches able to provide a compact representation of their underlying structure. These approaches aim at making the information content of a data set with, let's say, 100 coordinates, human readable and useful.

A possible route to achieve this goal is attempting to map the data on a two or three dimensional surface, which can then be visualized directly. This approach is followed in Principal Component Analysis [1] and, within a framework which allows taking non-linearities into account, in Diffusion Maps [2], Locally Linear Embedding [3], Tree Preserving Embedding [4] and Sketch-Map [5]. However, the intrinsic dimensionality (ID) of realistic data sets is often larger than three. This has become more and more evident in recent years, thanks to the development of powerful and accurate approaches capable of estimating the ID [6–8]. If the ID of a data set is, say, 10, any attempt to describe it with only two or three coordinates unavoidably leads to an information loss, making the above-mentioned methods only partially feasible in case of large IDs.

A different strategy for summarizing the information content of a data set is considering the data as an ensemble of realizations drawn from a probability distribution. The scope is then to find the peaks of this distribution and estimate their properties, for example, by using density-based clustering [9–12], without forcing the data onto a lower-dimensional representation. Importantly, this approach can be followed whatever the intrinsic dimensionality of the data set is. Moreover, it can also be exploited to build a hierarchical representation of the probability distribution, by seeking to build

a hierarchy of connected subsets of points. This idea was introduced in the seminal work of Hartigan [13] and has been exploited in many recent algorithms like, for instance, HDBSCAN [14], Robust Single Linkage [15] and Robust Density-Based Clustering [16].

In this work we introduce a method for reconstructing what we call the *topography* of a data set, namely a simplified human-readable chart of the probability distribution, conveying information on the height of all the probability peaks as well as on the organization of these peaks in larger structures. This chart provides immediate visual information not only about the clusters, but also about their relationships with each other. If the probability distribution includes N peaks, the topography consists in a $N \times N$ symmetric matrix, in which the diagonal entries are the heights of the peaks and the off-diagonal entries are the heights of the saddle points separating these peaks. An entry is equal to zero if the two peaks are not in contact. This matrix can be represented in the form of a tree diagram, like in references [13–16], a chart that unveils the hierarchies by focusing on the highest saddles between clusters. More in general, we will show that the topography can be visualized by one of the approaches developed for representing the kinetic models derived by Markov State Model analysis [17].

The topography is reconstructed by using a modified version of the Density Peaks (DP) algorithm [12]. This approach provides an empirical criterion for a quick and reliable localization of the density peaks. However, its original formulation is affected by two main drawbacks. First, the selection of cluster centers is relatively subjective, since it is based on the visual inspection of the so-called decision graph. Second, like all density-based clustering approaches, it is sensitive to the parameters involved in the density estimation [18]. These drawbacks have been addressed in many works [19–25]. For instance, Liang and Chen [23] automatically finds the number of clusters through a recursive inspection of the

* laio@sissa.it

† alexrod@sissa.it

decision graph based on a Divide-and-Conquer strategy. In the two-dimensional case, [22] proposes instead a non-parametric technique for estimating the densities based on the heat diffusion equation. Although the proposed method still requires the inspection of the decision graph, it shows an improved performance in the classification of artificial data sets. In Du *et al.* [20] it is proposed to estimate the density by a combination of Principal Components Analysis and the k-nearest neighbors method, while Wang and Xu [21] proposes a local density estimation based on a nonparametric multivariate kernel estimation, which measures the cutoff distance by a statistical approach. Extensions of the DP method are also available to address the propagation of errors in the assignment strategy, especially in data sets with highly overlapping clusters. In [24], for example, the authors propose an assignment strategy based on fuzzy weighted K-nearest neighbors, which makes the algorithm more robust to outliers. However the choice of the number of nearest neighbors k is not automatic and should be specified by the user. Along the same line, in [25] it is proposed a procedure to detect overlapping clusters in social networks, making the DP algorithm more reliable for studies in that field.

In this work we demonstrate that DP clustering algorithm can be made fully unsupervised and parameter-free by combining it with a non-parametric density estimator [26] recently proposed by us. This estimator is able to find by a statistical approach the largest region around each point in which the density is approximately constant. One of the main innovations with respect to other non-parametric estimators is that it measures the density in the manifold in which the data lay, and not in the embedding space whose dimensionality is normally overwhelmingly large. We will show that the mathematical formulation of the estimator in [26] naturally induces a simple criterion to automatically find the density peaks thorough the DP clustering. Moreover, the estimator provides a measure of the uncertainty on the density. This last feature is a key ingredient, since it allows to recognize genuine density peaks from statistical fluctuations due to finite sampling. Furthermore, it allows assessing the statistical reliability of the probability peaks which are recognized as genuine. This, to the best of our knowledge, is an original contribution of this work.

Finally, after testing the approach in several toy problems, we analyze two real world data sets: the MNIST database [27] of handwritten digits and a sample of protein sequences extracted from the Pfam clan PUA [28, 29], a complex superfamily organized into ten families, each containing a variety of architectures.

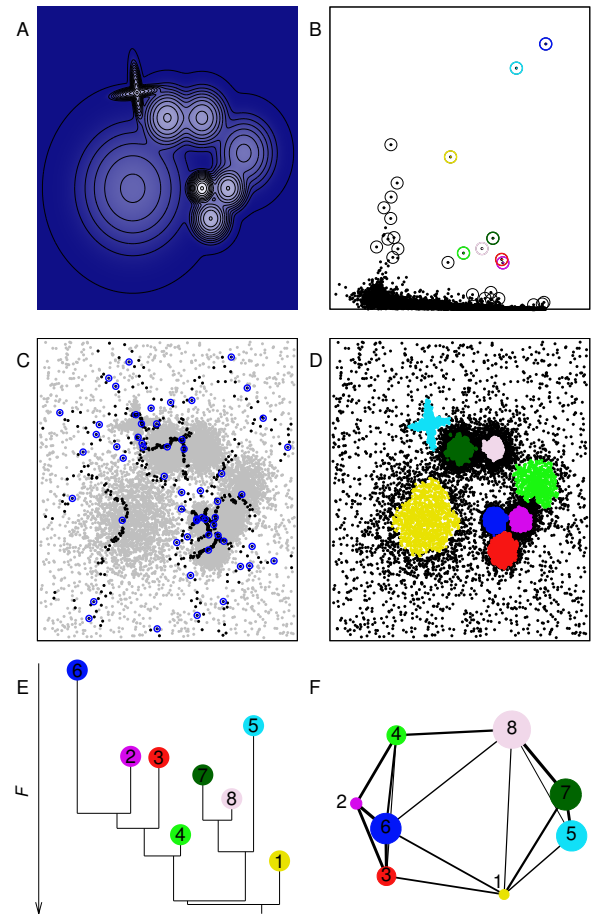


FIG. 1. Two dimensional toy examples. (A) Probability density function from which the 20000 points have been drawn. (B) Decision graph using g as density. Circled points correspond to the putative centers chosen by the automatic procedure described in section II A 2, while the colored ones are the centers of the significant clusters. (C) Borders (black points) and saddles (blue points) between clusters. (D) Final assignation of the points to clusters, black points correspond to halo points, while the color code is the same for panels B, E and F. (E) Dendrogram representation of the data set topography. (F) Network representation of the data set topography.

II. METHODS

A. Topography of Probability density function landscapes

Data sets can often be described as realizations of an underlying probability density function. This probability density is defined in the space of the coordinates of the data, and is often characterized by the presence of several maxima, at times organized hierarchically. A synthetic example of a probability density distribution with these features is shown in FIG. 1A.

The scope of our approach is reconstructing in an un-

supervised manner the topography of probability distributions characterized by those features. A key step of this procedure is identifying the density maxima within the data set and the saddle points between them. We will show that the density peaks and saddle points can be automatically recognized by making use of the PAk density estimator [26] within the framework of Density-Peak clustering [12]. In the following, we first summarize the principles of the PAk density estimator.

1. An adaptive k -Nearest Neighbor density estimator

PAk, which stands for Point Adaptive k -nearest neighbor, relies on the observation that, at constant density and for a given point i , the volumes of the shells defined by two successive nearest neighbors are independent and identically distributed according to an exponential distribution [8]. In this way, the k -NN estimation of the density is the maximum of the log-likelihood

$$\mathcal{L}_{i,k}(\rho) = k \cdot \log \rho - \rho \sum_{l=1}^k v_{i,l} = k \cdot \log \rho - \rho V_{i,k}. \quad (1)$$

where $v_{i,l} = \omega \left(r_{i,l}^d - r_{i,l-1}^d \right)$, where $r_{i,l}$ denotes the distance from the point i to the l -th neighbor and ω is a constant. The parameter d entering the equation is the Intrinsic Dimension (ID) of the manifold in which the data points lay. In the PAk approach one defines the likelihood using this parameter, rather than the dimension of the embedding space, which can be much larger than d . The variance associated with the maximum likelihood estimate decreases with the square root of k , so the estimate improves when using high values of k *if the density is constant*. PAk aims to find, for each data point, the largest neighborhood at which the density can be considered as constant by performing a Likelihood Ratio Test [30] between two models: a first one in which the densities at the point and at its k^{th} nearest neighbor are considered different and a second model in which the densities are the same. This test is applied to increasing values of k until the log-likelihoods of the two models are distinguishable with a very high statistical confidence ($p\text{-value}=10^{-6}$). Since it is likely that, with such degree of confidence, when the procedure stops the densities are already different, a linear correction is applied in order to deal with the induced bias. In detail, the rate of the exponential distribution is substituted by an *ansatz* in which the logarithm of the density at each of the sampled points varies linearly as one moves further and further from it. The modified likelihood is then maximized with respect to its free parameters by the Newton-Raphson approach. The error on the logarithm of the density is estimated from the variance of the likelihood, and it is given by $\varepsilon_i = \sqrt{\frac{4 \cdot \hat{k}_i + 2}{(\hat{k}_i - 1) \cdot \hat{k}_i}}$.

2. Automatical detection of density peaks

As in standard Density-Peaks clustering we here assume that the density peaks are surrounded by neighbors with lower local density and are at a relatively large distance from any points with a higher local density. However, the PAk estimator provides important additional information besides the density, which can be exploited for our analysis: an estimate of the error in the density and the neighborhood around each point in which the density can be considered approximately constant.

To find the density peaks we do not directly consider the density of points, which typically varies by several orders of magnitude, but the logarithm of their density $\log(\rho_i) = -F_i$, identified as the free energy at point i . Moreover, since the estimate of F can be affected by non-uniform errors, we define as cluster centers the local maxima of g_i , where g_i is defined as:

$$g_i = \log(\rho_i) + \varepsilon_i = -F_i + \varepsilon_i. \quad (2)$$

This definition is a generalization of the one used in [12], since the local maxima of g_i coincide with the local maxima of ρ_i if the error is uniform. If the error is not uniform, points with large error are less likely to be selected as local maxima with respect to points with a small error. Following reference [12] we then compute $\delta_i = \min_{j: g_j > g_i} r_{ij}$, namely the distance to the nearest point with higher g . In order to automatically find the cluster centers, we exploit an important property of the PAk density estimator that provides an estimate of the size of the neighborhood in which the logarithm of the density can be considered constant. Therefore, we consider as putative centers all the points for which

$$\delta_i > r_{\hat{k}_i} \quad (3)$$

where \hat{k}_i is the optimal number of nearest neighbors defined as in [26]. Thus, a data point i is a center only if all its \hat{k} nearest neighbors contributing to determine the value of its density have a value of g lower than g_i . A further check, which makes putative centers selection more robust in front of statistical fluctuations in the neighborhood estimation, is that a center can not belong to the neighborhood of any other point with higher g .

In Panel 1B we show the decision graph for a sample of 20000 points extracted from the probability density distribution shown in Panel A. The points surrounded by a circle are those that are automatically chosen as putative centers according to the criterion in (3).

The next step is to assign all the points that are not centers to the same cluster as the nearest point with higher g . This assignation is performed in order of decreasing g .

Choosing as centers the points highlighted in Panel 1B leads to a high splitting of the data set (see FIG. S1 for the result of this preliminary assignation). Indeed, the

criterion in (3) correctly identifies the genuine probability peaks but also the spurious statistical fluctuations of the density induced by the finite sampling.

In the following we describe a protocol that allows distinguishing meaningful density peaks from statistical fluctuations of the density.

3. Finding the saddle points

We here introduce a procedure that allows finding the saddle points between each peak and its neighboring peaks. We first find the data points that are at the border between two clusters. A point i , belonging to cluster c , is assumed to be at the border between cluster c and c' if its closest point j belonging to c' is within a distance r_{k_i} and if i is the closest point to j among those belonging to c . The saddle point between a pair of clusters c and c' is defined as the point with the highest value of g among those at the border between c and c' . The value of the logarithm of the density of this point and its error are denoted by $-F_{cc'}$ and $\varepsilon_{F_{cc'}}$. The border points between the clusters are shown in black in FIG. 1C, while the saddle points are circled in blue.

4. Assessing the peaks significance

Based on the value of the saddle free energies $F_{cc'}$ and their error we introduce a criterion for distinguishing genuine density peaks from statistical fluctuations of the density due to finite sampling. Qualitatively, if all the points in a cluster have density values compatible, within their errors, with the border density, the cluster can be considered as the result of a statistical fluctuation and merged with another cluster. In particular, cluster c is merged with cluster c' if

$$(F_{cc'} - F_c) < Z \cdot (\varepsilon_{F_c} + \varepsilon_{F_{cc'}}) \quad (4)$$

where $-F_c$ is the logarithm of the density of the center of cluster c .

The constant Z entering the equation fixes the level of statistical confidence at which one decides to consider a cluster meaningful. It is a free parameter of our approach, but its value has a clear statistical interpretation. In section II A 6 and in Supp. Inf. we will describe a criterion for choosing reasonable values of Z in real applications.

Condition (4) is checked for all the clusters c and c' in order of decreasing $-F_{cc'}$. This procedure allows pruning the set of clusters from those corresponding to density maxima that are not statistically robust, thus recovering the topography of the underlying probability function. Furthermore, the knowledge of the border densities between clusters allows finding the so-called halo, namely the set of points whose assignation is not reliable [12]. We here define as halo the points whose density is lower than the density of the lowest saddle point.

In FIG. 1D it can be seen that the cluster assignation after merging (with $Z = 1.5$) resembles almost perfectly the peaks shown in panel A (black points correspond to halo). Indeed, these results correspond with those obtained by the standard Density Peaks method choosing as centers the colored circles in panel B.

5. Representing the topography

The information about the location and the height of the saddles allows building a compact representation of the topography of the probability distribution function from which the data points are harvested.

To visualize the topography of the density distribution we follow two paths out of the several possibles. Both are based on the fact that the higher the density of the border between clusters, the higher can be considered the similarity between them. Therefore, we define the distance between two clusters as follows: $d_{cc'} = F_{cc'} - \min(F_c, F_{c'})$.

One possible way to visualize the topography is constructing a hierarchical tree by applying the Single Linkage algorithm [31] using these distances. In this case, the representation is similar to the one used in hierarchical density based methods [13–16]. In our case, to encode more information when representing the tree, the height of the branches is proportional to the density of the peak associated to them and the separation between branches in the x-axis is proportional to the population of the clusters. An example of this representation is provided in FIG. 1E.

An alternative way of representing the topography is projecting the clusters in two dimensions and visualizing their relationship as a network, where the thickness of the links between clusters is proportional to the log-density at the border. This brings to a representation similar to those used in Markov State Model analysis [17]. An example of this representation is provided in FIG. 1F. To encode more information in a single representation, the area of the disks representing the clusters is proportional to their population.

Both images provide complementary information about the underlying probability density function. In the example of FIG. 1 the hierarchical relationship between clusters 2, 3 and 6 (magenta, red and blue) is more evident in the tree representation. However, the close contact between clusters 4 and 8 (light green and light pink) is evident only using the network representation.

Additional test cases in several toy problems can be seen in S.I (FIG. S2-5).

6. Statistical significance of the clusters

The value of Z in (4) is used to control the statistical reliability of the density peaks. A more detailed analysis

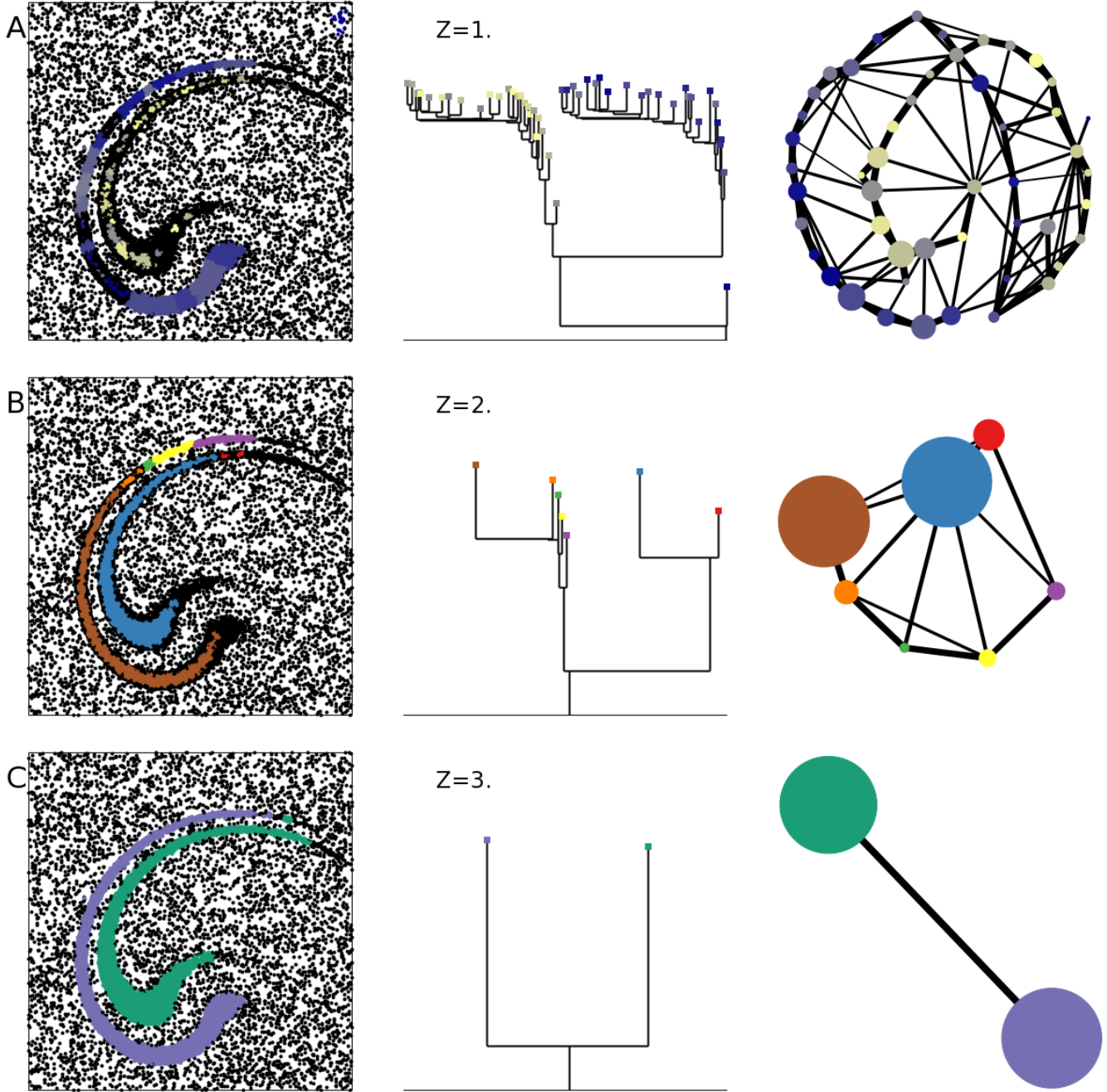


FIG. 2. Results of the topography reconstruction of a data set with two spirals at different values of Z (panel A, $Z = 1$, panel B $Z = 2$, and panel C $Z = 3$). The colors in the dendrogram (center) and in the network (right) correspond to those in the assignation (left).

of the role of this parameter can be found in Supplementary Text S1 and FIG. S6.

In general, at low Z values the method is more sensitive to variations of the density, but also identifies as clusters density fluctuations due to sampling artifacts. Then, the higher the value of Z , the lower the sensitivity to density changes but the higher the statistical reliability of the peaks. If the sampling of the probability distribution

function is good enough, one can increase the value of Z in order to enhance the statistical confidence. If the sampling is poor (something that easily happens if the intrinsic dimension of the data is high), one is forced to accept a lower level of confidence and a significant probability of observing some spurious clusters. In FIG. 2 we show an example of how the parameter Z affects the clustering classification in a well sampled distribution.

Although the best results are obtained with $Z = 3$, and the number of clusters increases for smaller Z , the topography of the data set allows identifying the two main peaks of the distribution at any value of the parameter Z .

III. RESULTS

A. Clustering a handwritten digits data set

We first tested our approach on the MNIST [27] data set, which includes 60000 images of handwritten digits between 0 and 9. We compute the pairwise distances with the tangent distance method [32]. The intrinsic dimension of the data set, estimated by the TWO-NN approach [8], is 8. The value of Z is set to 1.6. The results are summarized in FIG. 3, while the topography description is represented by the dendrogram in the left panel and by the network at the bottom.

The color of each cluster in the topography representations derives from a majority rule assignation, i.e. the color is the one corresponding to the label with higher presence in the cluster whose color code is indicated under the matrix. As it can be seen, although the network presents a quite high complexity, the splitting of labels into clusters is consistent with the ground truth classification. This complexity is due to the presence of elements whose employed distance can not capture the difference in the ground truth. In fact, the two main inconsistencies in the matrix come from cluster 1, where there is a mix of elements labeled as one, two or seven, and cluster 14, where the mixed labels are four and nine. A visual inspection confirms that elements in both clusters are similar enough to make it difficult to appreciate differences even for humans (see Fig. S7 for some examples). With the aim of quantifying the correspondence between the clustering and the ground truth classification, we assigned to each cluster a label with a majority rule and then we computed the Normalized Mutual Information (NMI) obtaining a value of 0.84. The confusion matrix for this comparison is shown in Table I.

| | 0 | 1 | 2 | 3 | 4 | 5 | 6 | 7 | 8 | 9 |
|----------|-------------|-------------|-------------|-------------|-------------|-------------|-------------|-------------|-------------|-------------|
| 0 | 5893 | 0 | 42 | 2 | 3 | 5 | 14 | 1 | 11 | 10 |
| 1 | 4 | 5032 | 141 | 8 | 34 | 3 | 21 | 44 | 48 | 3 |
| 2 | 0 | 1688 | 5699 | 304 | 15 | 58 | 1 | 1117 | 36 | 22 |
| 3 | 5 | 0 | 16 | 5690 | 1 | 104 | 1 | 0 | 115 | 54 |
| 4 | 2 | 6 | 3 | 1 | 5405 | 9 | 3 | 21 | 42 | 1065 |
| 5 | 3 | 0 | 2 | 46 | 0 | 5089 | 9 | 0 | 91 | 12 |
| 6 | 12 | 5 | 13 | 5 | 19 | 82 | 5867 | 0 | 34 | 1 |
| 7 | 0 | 5 | 32 | 22 | 7 | 6 | 0 | 5048 | 7 | 51 |
| 8 | 1 | 3 | 4 | 28 | 2 | 8 | 1 | 0 | 5374 | 14 |
| 9 | 3 | 3 | 6 | 25 | 356 | 57 | 1 | 34 | 93 | 4717 |

TABLE I. Confusion matrix between ground truth and cluster classification labeled according with a majority rule.

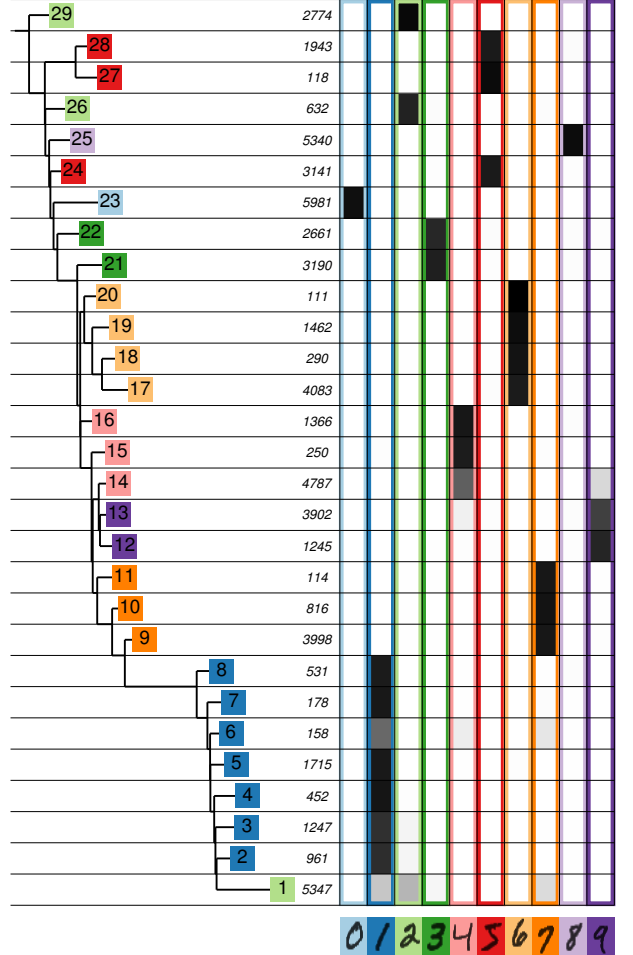
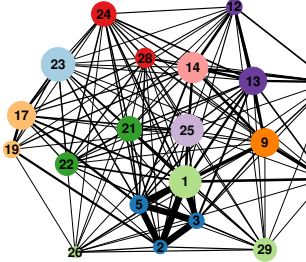


FIG. 3. Cluster analysis of the MNIST data set. In the matrix we represent, for clusters with a population greater than 100, the fraction of elements assigned to a cluster belonging to each of the ground truth labels. The higher the fraction, the darker the cell. On the left we show the dendrogram of the clusters. In correspondence to each leaf we indicate the cluster label and its population. To simplify the interpretation, the color of the background of the cluster is chosen according with a majority rule. For visualization purposes, only clusters with population higher or equal than 100 are shown. Bottom: the clusters with population higher than 600 in a network representation.



A further analysis of this data set was done after undersampling it. In this case, only 10000 out of 60000 images were analyzed. The computed intrinsic dimension with TWO-NN [8] is equal to 7, a result that is coherent with the loss of information due to the undersampling. In this case, the parameter Z is set to 1.0 since, as discussed above, to achieve a sufficient sensitivity to data structures one must lower the level of confidence, and accept a higher number of spurious clusters. The results are very similar to those of the complete data set. The main difference is that the mixing between the classes of number 4 and 9 is more significant, leading to a lower NMI of 0.76. The corresponding confusion matrix can be seen in Table S1.

B. The density topography of the PUA proteins clan

We finally exploit the approach introduced in this work to reconstruct the density topography of a sample of 9684 sequences extracted from the Pfam clan PUA. The Pfam database [28] is a large collection of protein families, grouped into clans or superfamilies; PUA is a complex superfamily organized into ten families with a population ranging from a few hundreds to thousands proteins. Many families contain a variety of protein architectures.

We first compute the local pairwise distances between the sequences by a BLAST [33] pairwise alignment. The intrinsic dimension of the data set estimated by TWO-NN [8] is equal to 9. If one uses the standard k -NN density estimator to cluster the PUA protein sequences the choice of the optimal global k is far from trivial. The PAk density estimator, not surprisingly, finds a huge variability in the optimal values for k , ranging from 3 to 170 across the data set, reflecting the complexity of the sample. Using the density estimated by PAk with Z equal to 2 one finds 123 clusters.

We test our results against the Pfam classification of PUA sequences into families, and going into greater detail, into architectures, by computing the purity of our clusters. Here the purity of a cluster C with respect to an architecture A is defined as the number of sequences in C belonging to A divided by the total population of C. In FIG. 4 we represent the correspondence between clusters ordered according to the dendrogram (y-axis) and architectures (x-axis). Again the network representation is shown at the bottom of the graph. Only architectures and clusters with a population greater than 40 are displayed. The Pfam denomination of the architectures considered in FIG. 4 is provided in Supplementary Material. In this representation the purity of clusters with respect to architectures is associated to a grey palette: the darker the cell, the higher the purity. FIG. 4 shows that clusters are substantially pure with respect to architectures (most of the clusters are over 90% pure). The quality of the results was also assessed by computing the NMI [34] of the clustering partition with respect to the

Pfam classification. Due to the hierarchical nature of the method, to compute the indices a family (or architecture) label is assigned to each cluster according to a majority rule. We find a NMI of 0.978 for the classification in families, and of 0.871 for the classification in architectures. This reveals a high degree of similarity between the clustering partition and the Pfam classification. The dendrogram provides further information on the complex topography of the data set, showing, for instance, that clusters belonging to the same architecture are closely related to each other. It essentially reflects the similarity between families in the clan as well as their division into architectures. The only important exception is that cluster 9 is divided between families TruB-C.2 and TruB-C. These two families are characterized by a low similarity in the sequences within the same family. Thus the error in the estimated densities is so large that the faint saddle point that separates the two families is classified by our algorithm as a statistical fluctuation.

The network representation shows a complex landscape. For instance, while some families are well isolated others are interconnected through one or several nodes. The families PUA and LON are divided in many clusters but they are densely interconnected between them. On the contrary, the family ASCH, although connected, appears to be quite sparse. The centrality of cluster 9 between families TruB-C.2 and TruB-C is in agreement with the analysis of the dendrogram.

IV. DISCUSSION

In this work we introduce a tool for analyzing large and multidimensional data sets. Our tool is specifically designed to treat cases in which the standard projection technique (e.g. PCA) gives poor results. The idea is reconstructing the *topography* of the probability distribution from which the data are harvested. This topography is a list of probability peaks, each characterized by its properties: the height of the probability maximum, the population, the list of neighboring peaks, etc. The topography is estimated using only the distance between points, avoiding the use of any coordinate system or projection. We illustrated two manners of visualizing this topography: a hierarchical representation equivalent to the one used in [13–16] and a graph representation tantamount to the one of Markov State Models [17]. Of course, one can imagine other graphical representations.

The topography is reconstructed by a modified version of the Density Peaks clustering algorithm [12], which is parameter free and unsupervised. A key ingredient of this modified algorithm is the PAk density estimator, which provides an accurate estimation of the probability density at the data points in the manifold that embeds them, as well as the error associated with the estimate. This error is used for assessing the statistical significance of the peaks found by the clustering procedure and, thus, to discriminate between real features of the underlying

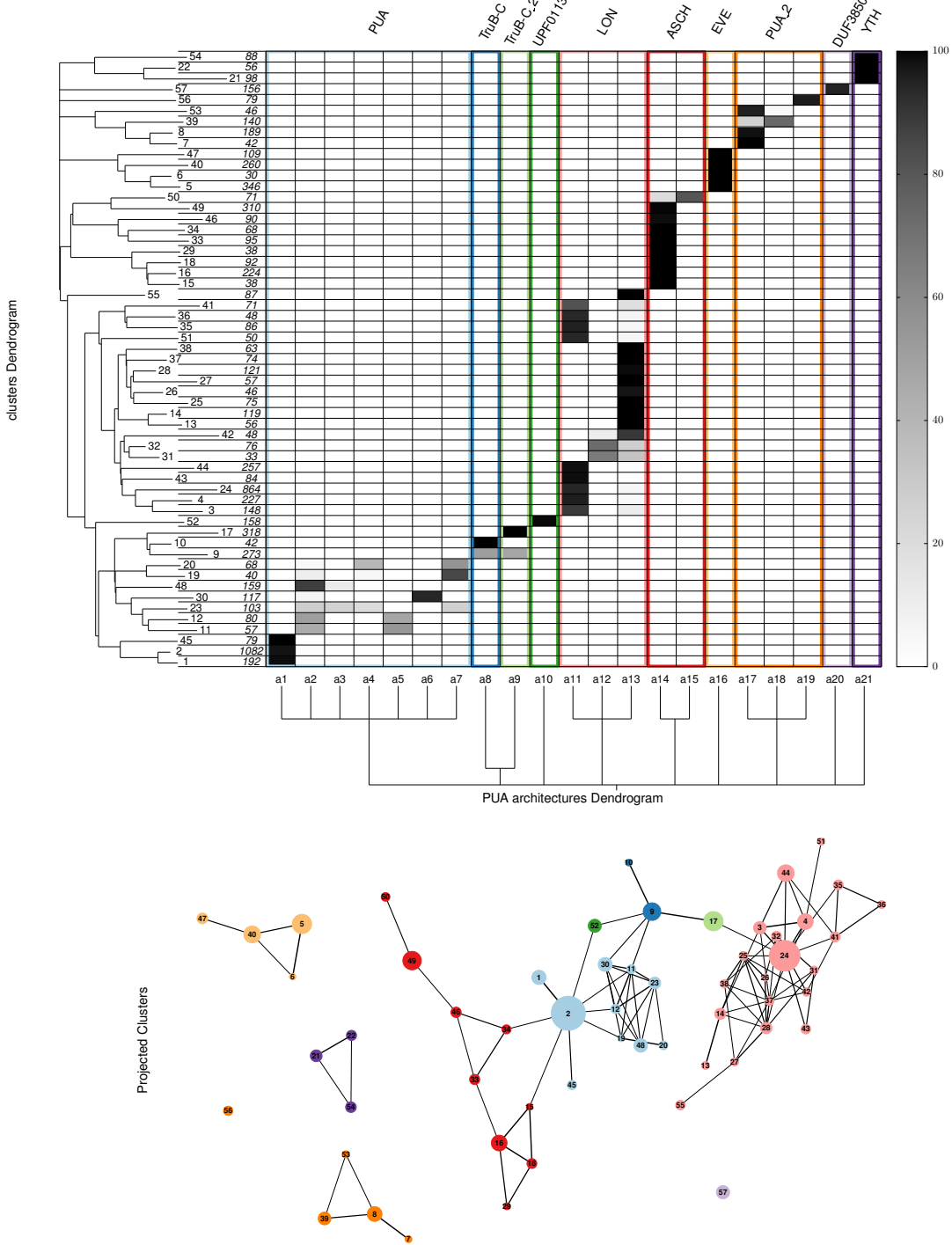


FIG. 4. Cluster analysis of the clan PUA from the Pfam database. We represent the Purity Matrix for clusters and architectures with a population greater than 40. Color boxes correspond to families. The purity of the clusters with respect to architectures is associated to a grey palette: the darker the cell, the higher the purity. On the left of the Purity Matrix we show the dendrogram of the clusters. In correspondence to each leaf we indicate the cluster label and the population of the cluster. The dendrogram at the bottom is a schematic visualization of the hierarchical relationship existing between architectures according to Pfam: architectures connected at a higher level (e.g. a1, a2, a3) belong to the same family, while those connected at a lower level (e.g. a12, a13) belong to a clan. The Pfam denomination of the architectures is provided in Supp. Inf. .Bottom: the clusters represented in the top panel in a network representation.

probability distribution function and sampling artifacts due to the finite sampling.

The statistical reliability of the probability peaks is quantified by the Z score, which qualitatively measures the negative of the probability that the peak is generated by a statistical fluctuation. By choosing a threshold on Z , one can filter out the peaks that are less reliable, and obtain a more compact representation of the data.

The computational scaling of the method is determined by the search of the nearest neighbors in the PAk algorithm whose brute force implementation is $O(N^2)$, since the nearest neighbor search requires computing the whole distance matrix. However, there are approaches that could lower this complexity to $O(N \log(N))$ [35].

The method performs well in the two dimensional toy

examples in FIG. 1 and 2. However, it shows its real power when the number of features is huge, as in the cases of the handwritten numbers and the PUA family, where computing the density in the manifold that embeds the data instead of computing it in the coordinate space is a key for a successful reconstruction of the topography. Moreover, the use of PAk coupled with the Density Peaks clustering algorithm leads to an accurate detection of the main features of the underlying probability distribution whose statistical reliability can be assessed from the parameter Z . Furthermore, the knowledge of the density at the borders permits the visualization of the relationship between these modes –the topography– in several ways providing a visual grasp of the structure of the data set with an unprecedented level of detail.

[1] M. Ringnér, *Nature biotechnology* **26**, 303 (2008).

[2] R. R. Coifman, S. Lafon, A. B. Lee, M. Maggioni, B. Nadler, F. Warner, and S. W. Zucker, *Proceedings of the National Academy of Sciences of the United States of America* **102**, 7426 (2005), <http://www.pnas.org/content/102/21/7426.full.pdf>.

[3] S. T. Roweis and L. K. Saul, *Science* **290**, 2323 (2000), <http://science.sciencemag.org/content/290/5500/2323.full.pdf>.

[4] A. D. Shieh, T. B. Hashimoto, and E. M. Airoldi, *Proceedings of the National Academy of Sciences* **108**, 16916 (2011), <http://www.pnas.org/content/108/41/16916.full.pdf>.

[5] M. Ceriotti, G. A. Tribello, and M. Parrinello, *Proceedings of the National Academy of Sciences* **108**, 13023 (2011), <http://www.pnas.org/content/108/32/13023.full.pdf>.

[6] F. Camastrà and A. Staiano, *Information Sciences* **328**, 26 (2016).

[7] D. Granata and V. Carnevale, *Scientific reports* **6**, 31377 (2016).

[8] E. Facco, M. d'Errico, A. Rodriguez, and A. Laio, *Scientific reports* **7**, 12140 (2017).

[9] M. Ester, H.-P. Kriegel, J. Sander, and X. Xu, in *Second International Conference on Knowledge Discovery and Data Mining*, Vol. 96, edited by E. Simoudis, J. Han, and U. M. Fayyad (AAAI Press, 1996) pp. 226–231.

[10] M. Ankerst, M. M. Breunig, H.-P. Kriegel, and J. Sander, *SIGMOD Rec.* **28**, 49 (1999).

[11] D. Comaniciu and P. Meer, *IEEE Transactions on Pattern Analysis and Machine Intelligence* **24**, 603 (2002).

[12] A. Rodriguez and A. Laio, *Science* **344**, 1492 (2014), <http://science.sciencemag.org/content/344/6191/1492.full.pdf>.

[13] J. A. Hartigan, *Journal of the American Statistical Association* **76**, 388 (1981).

[14] R. J. Campello, D. Moulavi, and J. Sander, in *Pacific-Asia Conference on Knowledge Discovery and Data Mining* (Springer, 2013) pp. 160–172.

[15] K. Chaudhuri, S. Dasgupta, S. Kpotufe, and U. von Luxburg, *IEEE Transactions on Information Theory* **60**, 7900 (2014).

[16] F. Sittel and G. Stock, *Journal of chemical theory and computation* **12**, 2426 (2016).

[17] V. S. Pande, K. Beauchamp, and G. R. Bowman, *Meth-*ods **52**, 99 (2010), *protein Folding*.

[18] D. Xu and Y. Tian, *Annals of Data Science* **2**, 165 (2015).

[19] W. Zhang and J. Li, *CoRR* **abs/1505.05610** (2015), [arXiv:1505.05610](https://arxiv.org/abs/1505.05610).

[20] M. Du, S. Ding, and H. Jia, *Knowledge-Based Systems* **99**, 135 (2016).

[21] X.-F. Wang and Y. Xu, *Statistical Methods in Medical Research* (2015), 10.1177/0962280215609948, <https://doi.org/10.1177/0962280215609948>.

[22] R. Mehmood, G. Zhang, R. Bie, H. Dawood, and H. Ahmad, *Neurocomputing* **208**, 210 (2016), si: BridgingSemantic.

[23] Z. Liang and P. Chen, *Pattern Recognition Letters* **73**, 52 (2016).

[24] J. Xie, H. Gao, W. Xie, X. Liu, and P. W. Grant, *Information Sciences* **354**, 19 (2016).

[25] M. Wang, W. Zuo, and Y. Wang, *Neurocomputing* **179**, 219 (2016).

[26] A. Rodriguez, M. d'Errico, E. Facco, and A. Laio, “Computing the free energy without collective variables,” (2017).

[27] Y. LeCun, L. Bottou, Y. Bengio, and P. Haffner, *Proceedings of the IEEE* **86**, 2278 (1998).

[28] R. D. Finn, A. Bateman, J. Clements, P. Coggill, R. Y. Eberhardt, S. R. Eddy, A. Heger, K. Hetherington, L. Holm, J. Mistry, E. L. L. Sonnhammer, J. Tate, and M. Punta, *Nucleic Acids Research* **42**, D222 (2014).

[29] R. D. Finn, P. Coggill, R. Y. Eberhardt, S. R. Eddy, J. Mistry, A. L. Mitchell, S. C. Potter, M. Punta, M. Qureshi, A. Sangrador-Vegas, G. A. Salazar, J. Tate, and A. Bateman, *Nucleic Acids Research* **44**, D279 (2016).

[30] J. Neyman and E. S. Pearson, *Philosophical Transactions of the Royal Society of London. Series A, Containing Papers of a Mathematical or Physical Character* **231**, 289 (1933).

[31] J. A. Hartigan, *Journal of the American Statistical Association* **76**, 388 (1981).

[32] P. Simard, Y. LeCun, and J. S. Denker, in *Advances in neural information processing systems* (1993) pp. 50–58.

[33] S. F. Altschul, W. Gish, W. Miller, E. W. Myers, and D. J. Lipman, *Journal of molecular biology* **215**, 403 (1990).

[34] N. X. Vinh, J. Epps, and J. Bailey, *J. Mach. Learn. Res.* **11**, 2837 (2010).

[35] M. Muja and D. G. Lowe, *IEEE Transactions on Pattern Analysis and Machine Intelligence* **36**, 2227 (2014).